

Elastic constants, electronic properties and thermoelectric response of LiAlX (X=C, Si, Ge, and Sn) half-Heusler compounds

M. Khetir^a, A. Maafa^a, F. Boukabrine^b, H. Rozale^{a,*}, A. Bouabça^a and A. Chahed^a

^aCondensed Matter and sustainable development Laboratory (LMCDD),
University of Sidi Bel-Abbes, Sidi Bel-Abbes 22000, Algeria.

*e-mail: hrozale@yahoo.fr; hrozale@univ-sba.dz

^bThe Study of Materials and Optical Instrumentation Laboratory (LEMIO),
University of Sidi Bel-Abbes, Sidi Bel-Abbes 22000, Algeria.

Received 23 April 2021; accepted 08 June 2021

Since they have become indispensable in various technological applications and a powerful source for generating energy in thermoelectric devices, Lithium-based alloys are the central topic of many experimental and theoretical reports. Hence, LiAlX (X = C, Si, Ge, Sn) materials represent the main research in this study. Different interesting properties such as the effect of pressure on the band gaps as well as the elastic parameters and the thermoelectric efficiency of these materials were investigated using the full potential linearized augmented plane wave (FP-LAPW) method. LiAlX alloys were found to be semiconducting with indirect band gaps. When studying the mechanical properties, we realized that LiAlC alloy remains stable against a wide range of pressure changes (90 GPa), while the rest three systems preserve their mechanical stability in a moderate range of 40, 50 and 30 GPa, respectively. The semiconducting band gap for each possible transition have been calculated in a range of different pressures using both GGA and mBJ-GGA approximations. The results revealed a decaying trend of the indirect gap along Γ -X direction with increase of pressure. High values of the power factor were achieved and a large figure of merit (almost 0.7 for all systems) was calculated at 600 K, which makes these Li-based alloys very auspicious in the thermoelectric field applications.

Keywords: Lithium-based alloys; DFT; FP-LAPW; elastic constants; electronic properties; thermoelectric response.

DOI: <https://doi.org/10.31349/RevMexFis.68.011002>

1. Introduction

After the discovery of half-metallicity in the half-Heusler NiMnSb [1], Heusler compounds having the XYZ phase have proved their efficiency in the most revolutionized fields of technology such as optoelectronics [2-5], spintronics [6-8], and thermoelectric applications [9]. These compounds are mainly inter-metallic materials that consist of transition metals (X and Y) and a main group (Z) element. They have a non-centrosymmetric structure (C1b) conforming to an F-43m space group (No. 216) [10] with Wyckoff positions 4a (0,0,0), 4b (1/2,1/2,1/2) and 4c (1/4,1/4,1/4). Half-Heusler compounds are formed in a crystal of the MgAgAs type structure as four interpenetrating face-centered cubic superlattices with type 1, type 2 or type 3 structural phases [11]. In this work, we have studied the effect of pressure on the band gaps, the mechanical stability at ambient conditions and under pressure in addition to the thermoelectric properties of four lithium based half-Heusler compounds using first principles calculations [12]. These Li-based systems have been determined to be semiconducting with indirect large and narrow band gaps. The effect of pressure on all elastic parameters have been investigated. LiAlX (X = C, Si, Ge, Sn) systems have proved to be stable at high values of pressures. They also possess a high figure of merit (ZT), which makes them very attractive candidates in the fields of photovoltaics [13] and thermoelectric device applications [14].

1.1. Computational details

Using the full-potential linearized augmented plane-wave (FP-LAPW) method [15-17] implemented in the WIEN2k package [18], we have calculated the electronic properties, magnetic structures, mechanical stability and thermoelectric properties of a series of LiAlX (X = C, Si, Ge, Sn) half-Heusler compounds. The electronic exchange-correlation energy was treated using the generalized gradient approximation parameterized by Perdew-Burke-Ernzerhof (GGA-PBE) [19,20]. In addition, the modified Becke-Johnson (mBJ) approximation [21] was employed to predict the band gaps more precisely. The total energy dependence on the cell volume was fitted to the modified Murnaghan equation of state [22].

The cut-off parameter RMT^*K_{\max} in the basis set was chosen to be 8 [23], where K_{\max} is the plane wave cut-off and RMT is the smallest muffin-tin radius. 2000 k -points have been used in the calculations, where the cut-off energy separating the core and the valence states was set at -6.0 Ry. For the elastic constants, we have employed the Thomas Charpin method [24]. While the thermoelectric properties were calculated using the Boltzmann theory as implemented in BoltzTrap code [25].

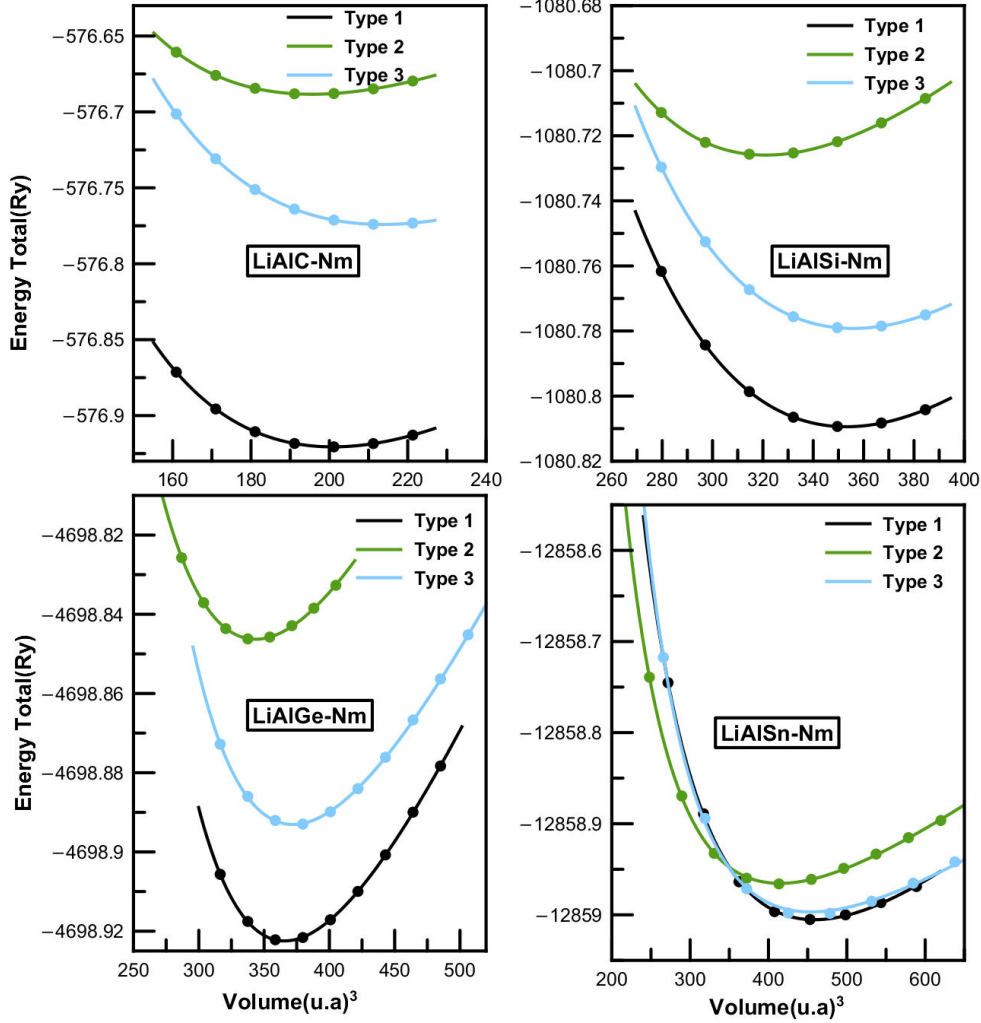


FIGURE 1. Volume optimization curves for LiAlX(X=C, Si, Ge, and Sn) compounds in Type 1, 2 and 3 half-Heusler structures in the nonmagnetic state.

TABLE I. The lattice constants (a_0), bulk modulus (B_0), pressure derivative of the bulk modulus (B'_0), equilibrium Volume, ground state energy $E_{FM} - E_{NM}$, and gap energy (eV) calculated for LiAlX (X=C, Si, Ge, Sn) alloys in comparison to some available experimental and/or theoretical results.

Compound	Type	$E_{NM} - E_{FM}$ (Ry)		a_0 (Å)	B_0 (GPa)	B'_0	$E_{NM} - E_{FM}$	Gap(eV)	
		NM	FM					NM	NM
LiAlC	1	-576.9193	-576.9183	4.91	127.4	3.69	10^{-3}	0.81	1.64
	2	-576.6792	-576.6892					0.81[34]	1.63[34]
	3	-576.7492	-576.7325						
LiAlSi	1	-1081.8077	-1081.8057	5.93	63	3.7	2×10^{-4}	0.11	0.49
	2	-1081.7311	-1081.7352					0.118[34]	0.51[34]
	3	-1081.7977	-1081.7975						
LiAlGe	1	-4698.9224	-4698.9223	6.01	55.8	3.91	1.3×10^{-4}	0.055	0.52
	2	-4698.8462	-4698.8562					0.053	0.52[34]
	3	-4698.8930	-4698.8931						
LiAlSn	1	-12859.0031	-12858.9995	6.47	42.88	3.56	3.5×10^{-3}	0.16	0.55
	2	-12858.9586	-12858.9584						
	3	-12858.9967	-12858.9961						

2. Results and discussion

2.1. Structural properties

The ternary half-Heusler compounds crystallize in three different structural phases labelled as Type 1, Type 2 and Type 3. These phases differ according to the positions of atoms in the cubic lattice structure. The optimal structural parameters of the LiAlX (X = C, Si, Ge, Sn) compounds were calculated in the nonmagnetic and ferromagnetic states for each structural phase. The total energy as function of the unit cell volume are shown in Figs. 1 and 2. We present as well the equilibrium lattice parameters, calculated band gaps, bulk modulus and its pressure derivative in Table I.

Both Figs. 1 and 2 show that Type 1 structure is the most stable among all the structural phases. Furthermore, the minimum energy corresponds to the nonmagnetic state, which indicates a paramagnetic behavior of the studied compounds. The remaining properties will be estimated for the Type 1 nonmagnetic most stable structure for all four Li-based systems.

The resulting lattice parameters are in good agreement with other published experimental data [26,27]. From Ta-

ble I, we notice that the lattice parameter increases downward in the Mendeleev periodic table from LiAlC to LiAlSn, while the bulk modulus decreases.

2.2. Mechanical properties

The study of the mechanical stability and durability of a crystal against applied forces is very important to determine the strength and resistivity of any material. The three independent elastic constants C_{11} , C_{12} and C_{44} of the cubic LiAlX (X = C, Si, Ge, Sn) structures were calculated at normal pressure and under hydrostatic pressure. The calculations of the stability criteria and the evolution of C_{ij} , bulk B , shear G and Young modulus E were also illustrated as function of pressure in Fig. 3. From this figure it can be observed that with the rise in compression the value of all elastic constants increases and we notice that the stability criteria are verified for all LiAlX alloys with changing pressure.

The constant C_{11} , related to the linear elasticity, increases with pressure, signaling that pressure enhances the tensile strength of all compounds. The C_{44} elastic constant, which is related to shape deformation, becomes less affected against rising pressures, indicating less bond strength enhancement.

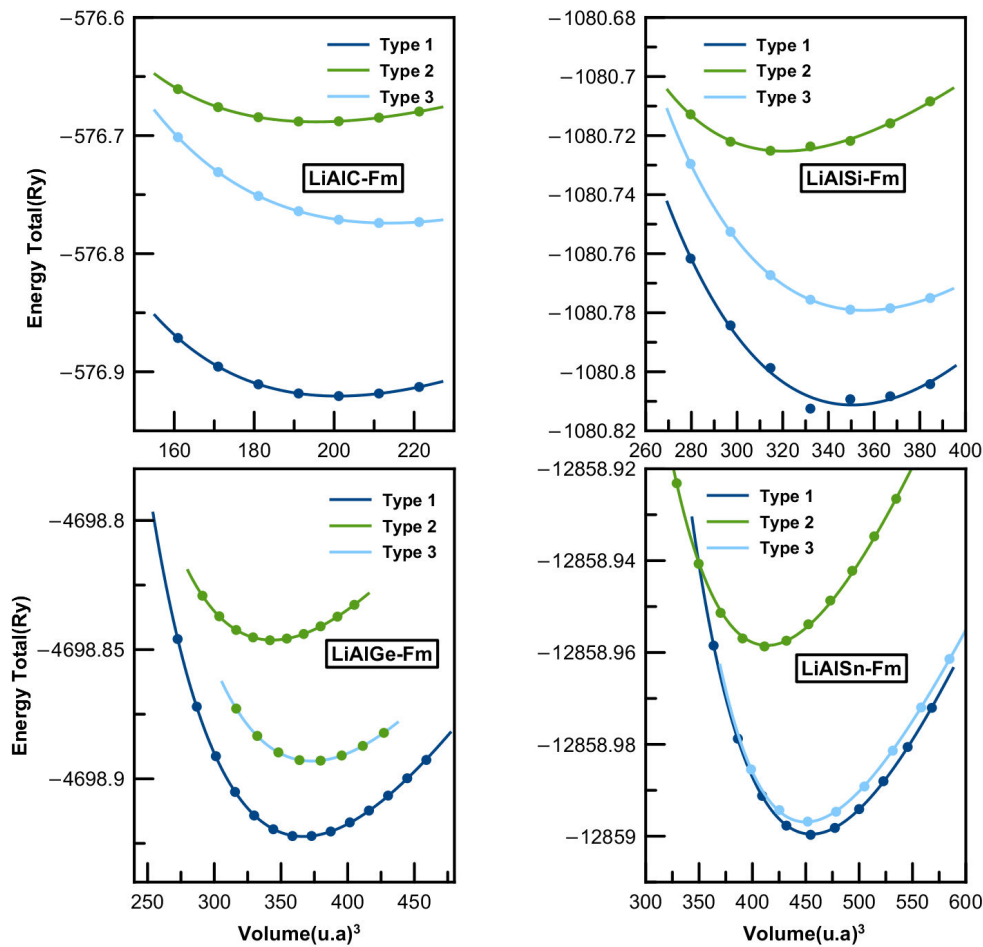


FIGURE 2. Volume optimization curves for LiAlX (X=C, Si, Ge, and Sn) compounds in Type 1, 2 and 3 half-Heusler structures in the ferromagnetic state.

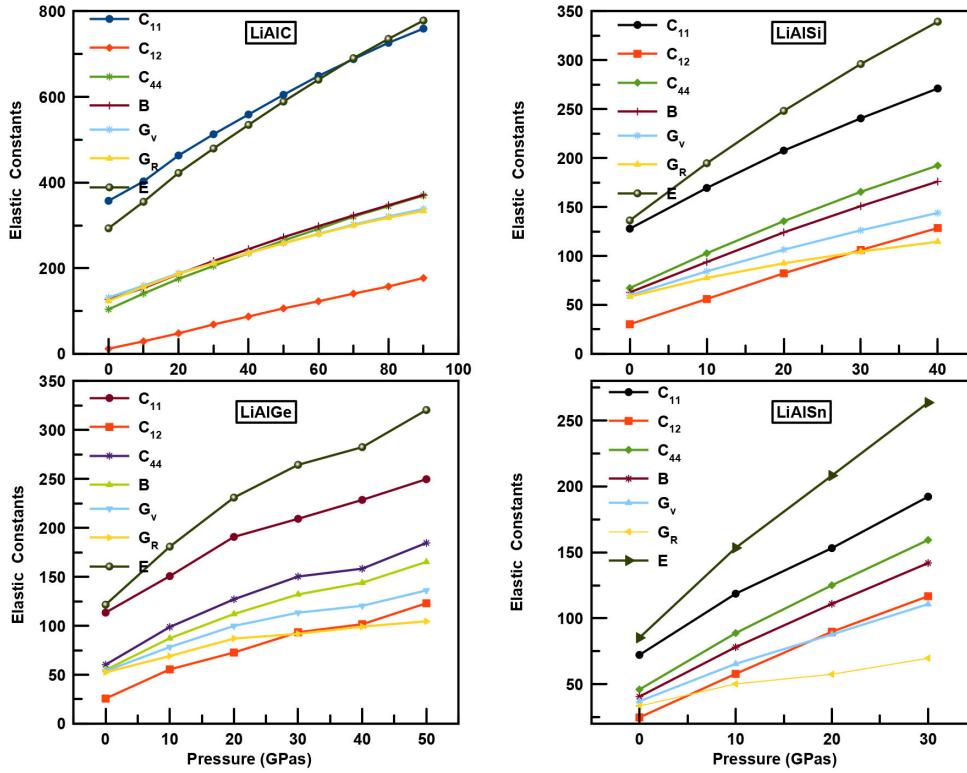


FIGURE 3. Variation of the elastic parameters as function of pressure for LiAlX (X= C, Si, Ge, Sn) alloys.

The stability of cubic systems at zero pressure can be studied using the Born-Huang stability conditions [28]

$$C_{44} > 0, \quad \frac{1}{2(C_{11} - C_{12})} > 0, \quad C_{12} < B < C_{11}.$$

However, Born's elastic stability criteria are inapplicable when the pressure is different from zero. The calculated values of the elastic constants under hydrostatic pressure were compared with the generalized stability criteria [29] using the following relations:

$$K = \frac{1}{3(C_{11} + 2C_{12} + P)} > 0,$$

$$G = \frac{1}{2(C_{11} - C_{12} - 2P)} > 0,$$

$$G' = C_{44} - P > 0.$$

Figure 4 shows the pressure dependence of the generalized stability criteria for LiAlX (X = C, Si, Ge, and Sn) compounds. Our calculations show that G' increases progressively with the pressure, while G decreases with pressure except for the compound LiAlC which remains approximately linear. These alloys are then mechanically stable and can maintain their stability along a wide range of pressures, especially LiAlC, which retains its structural stability in a pressure range of 0 to 90 GPa. In contrast, LiAlSi, LiAlGe and LiAlSn become unstable over a pressure superior of 40, 50 and 30 GPa, respectively.

From the elastic constants, we have derived the rest of the mechanical parameters. The bulk values of LiAlX alloys that were extracted from the Murnaghan equation of state are very close to the values calculated using the elastic constants at zero pressure for all alloys. It is well known that the shear modulus G represents the resistance of a material against plastic deformation, while Young's modulus Y [30] is associated with the stiffness of a solid. From Fig. 3, we notice that, at zero pressure, LiAlC has a larger shear modulus than the rest of materials, which confirms its high stiffness. By increasing the pressure, the values of G and E increase as well. In fact, the higher the pressure, the higher the stiffness of these materials as well as their resistivity against deformation.

The ductility and brittleness of a material is also explained by Pugh's ratio (k) defined by B/G [31]. A material is brittle if $B/G < 1.75$, otherwise it behaves as a ductile system. From the previous tables, it is evident that the four systems are brittle at ambient pressure. Even when increasing pressure, Pugh's ratio increases gradually but the brittle behavior is still dominant in all four alloys. The negative Cauchy pressure C_p ($C_{12} < C_{44}$) also confirms the brittle nature in these materials. Poisson's ratio serves in knowing the compressibility of a crystal as well as the bonding type (covalent or metallic bonding). For covalent bonding, Poisson's ratio is about $\nu = 0.1$, and it increases for ionic crystals up to $\nu = 0.25$ [32,33]. The resulting values of Poisson's ratio barely change (less than 0.2) with increase of pressure (see Fig. 5), which reflects the covalent characteristics of the

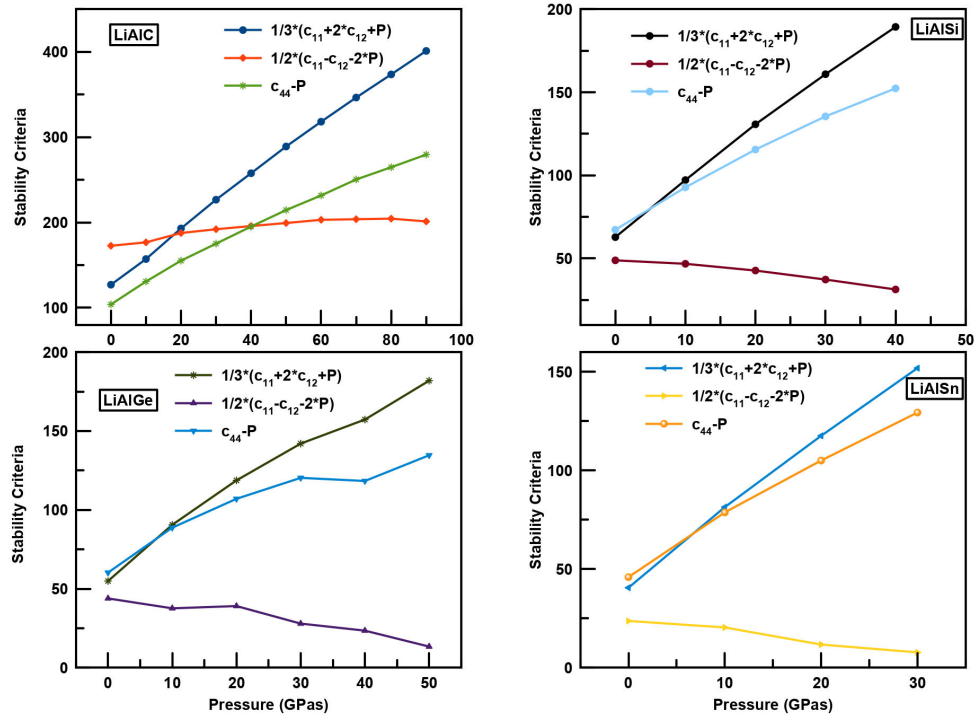


FIGURE 4. Generalized stability criteria as function of pressure for LiAlX (X= C, Si, Ge, Sn) alloys.

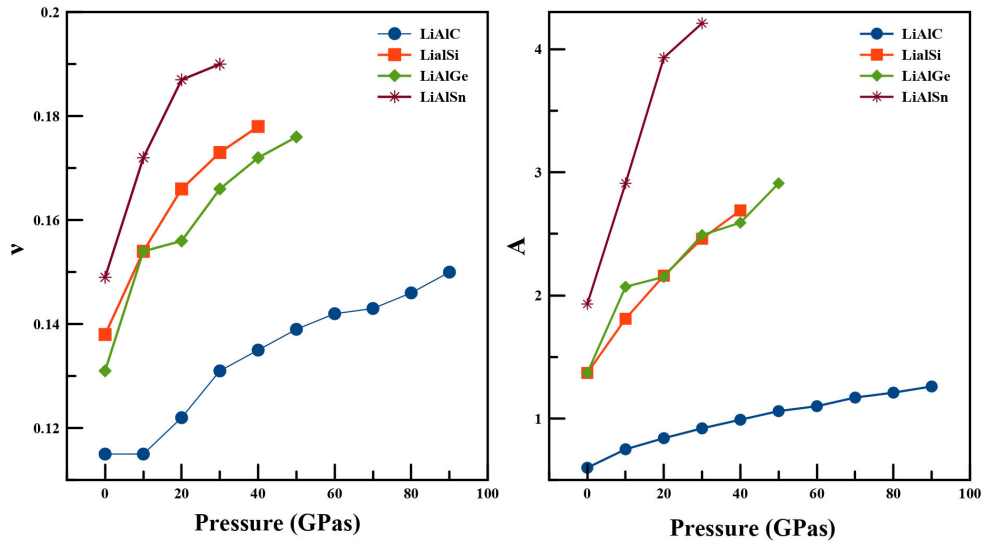


FIGURE 5. Variation of the Poisson's ratio ν and elastic anisotropy A as function of pressure for LiAlX (X= C, Si, Ge, Sn) alloys.

studied materials. Another important factor is the elastic anisotropy A [34], presented in Fig. 5, that correlates to the possibility of inducing micro-cracks during the growth of materials; a large value of A is related to the instability of the lattice structure. At ambient conditions, all alloys possess small values of shear elastic anisotropy. Following an increase of pressure, the values of A are not very much affected, which confirms the stability of the Type 1 structure. The anisotropy factor is also a measure of the degree of elastic anisotropy in solids and since the resulting anisotropy values are different

from unity, these systems can be considered as anisotropic. For LiAlSn, we notice that the values of A increase the most with increase of pressure as compared to the rest three compounds. This indicates that the degree of elastic anisotropy in this compound grows when the pressure increases.

2.2.1. Electronic properties

The band structures of the semiconducting LiAlX alloys are presented in Fig. 6, where an indirect band gap characterizes

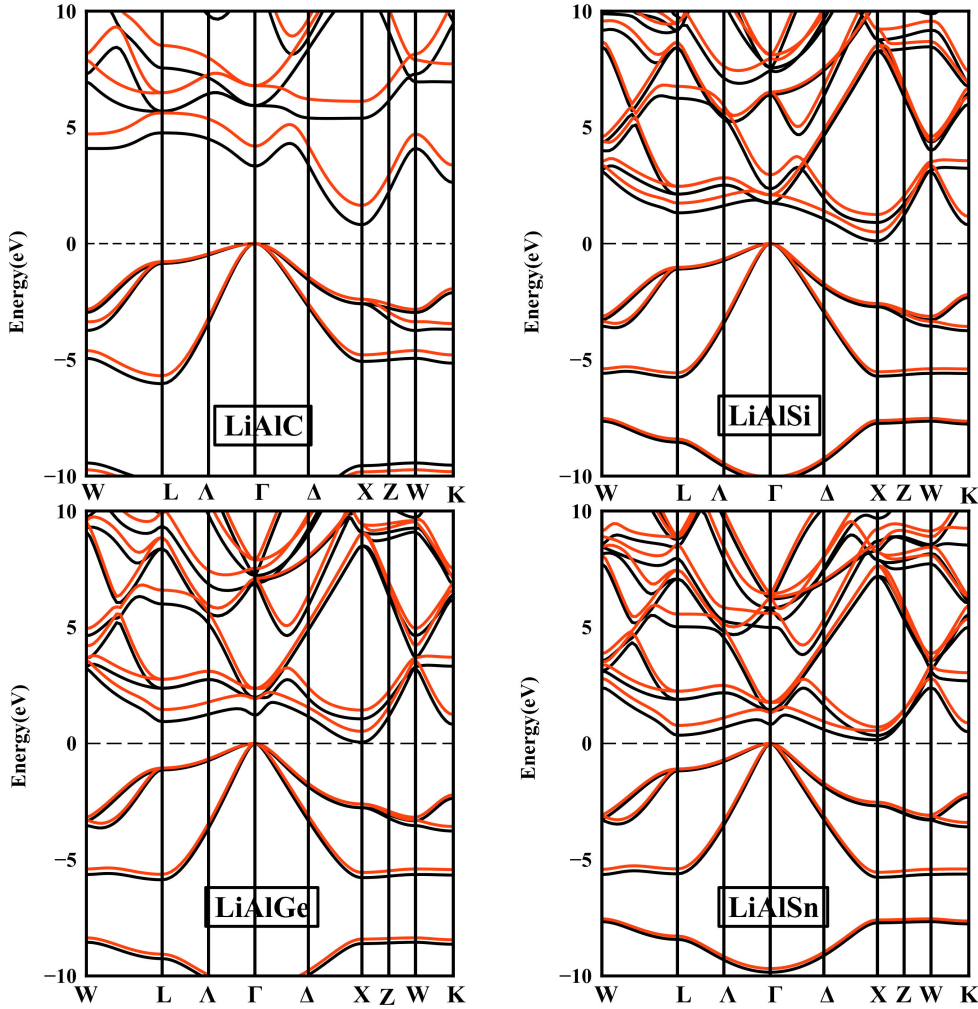


FIGURE 6. Electronic band structure in cubic (MgAgAs-type) phase for LiAlX (X=C, Si, Ge, Sn) alloys. The black lines represent GGA calculations and the red lines refer to the GGA-mBJ approximations.

TABLE II. Calculated energy band gaps (in eV) using the GGA and GGA-mBJ scheme for LiAlC.

LiAlC	GGA			GGA-mBJ		
	$\Gamma - X$	$\Gamma - \Gamma$	$\Gamma - L$	$\Gamma - X$	$\Gamma - \Gamma$	$\Gamma - L$
0	0.81	3.33	4.76	1.64	4.19	5.61
10	0.80	3.79	5.23	1.39	4.36	5.82
20	0.78	4.29	5.75	1.37	4.85	6.33
30	0.77	4.72	6.19	1.64	5.60	7.05
40	0.76	5.09	6.33	1.63	5.98	7.20
50	0.74	5.42	6.45	1.62	6.31	7.33
60	0.73	5.72	5.56	1.33	6.27	7.17
70	0.72	5.99	6.66	1.32	6.54	7.28
80	0.70	6.24	6.76	1.60	7.14	7.67
90	0.69	7.47	6.84	1.30	7.02	7.47

TABLE III. Calculated energy band gaps (in eV) using the GGA and GGA-mBJ scheme for LiAlSi.

LiAlSi						
	GGA			GGA-mBJ		
	$\Gamma - X$	$\Gamma - \Gamma$	$\Gamma - L$	$\Gamma - X$	$\Gamma - \Gamma$	$\Gamma - L$
0	0.11	1.74	1.32	0.49	2.09	1.74
				0.48 [27]	2.10 [27]	1.80[27]
10	-0.002	1.73	1.79	0.29	2.08	2.16
20	-0.015	1.70	1.96	0.01	1.95	2.19
30	-0.05	1.68	2.05	-0.012	1.93	2.12
40	-0.09	1.66	2.07	-0.03	1.90	2.05

TABLE IV. Calculated energy band gaps (in eV) using the GGA and GGA-mBJ scheme for LiAlGe.

LiAlGe						
	GGA			GGA-mBJ		
	$\Gamma - X$	$\Gamma - \Gamma$	$\Gamma - L$	$\Gamma - X$	$\Gamma - \Gamma$	$\Gamma - L$
0	0.055	1.20	0.93	0.52	1.92	1.45
				0.52[27]	2.15[27]	1.58[27]
10	-0.008	2.06	1.46	0.33	2.45	1.97
20	-0.016	2.11	1.79	0.21	2.51	2.30
30	-0.034	2.16	2.03	0.12	2.55	2.54
40	-0.048	2.18	2.16	0.07	2.57	2.67
50	-0.075	2.21	2.37	-0.02	2.61	2.74

TABLE V. Calculated energy band gaps (in eV) using the GGA and GGA-mBJ scheme for LiAlSn.

LiAlSn						
	GGA			GGA-mBJ		
	$\Gamma - X$	$\Gamma - \Gamma$	$\Gamma - L$	$\Gamma - X$	$\Gamma - \Gamma$	$\Gamma - L$
0	0.16	0.080	0.35	0.55	1.32	0.77
10	0.0	1.50	0.93	0.30	1.78	1.30
20	0.04	1.62	1.26	0.09	1.79	1.67
30	0.03	1.47	1.54	0.03	1.84	1.99

the four Li-based alloys, with the valance band maximum at Γ point and the conduction band minimum at X point. The resulting band gaps calculated for LiAlC, LiAlSi and LiAlGe with either GGA or mBJ-GGA are very close to other theoretical data [35]. For LiAlSn, no theoretical or experimental data were available to compare the structural parameters of this compound.

Along $\Gamma - X$ direction, the highest band gap was obtained for LiAlC with a value of 0.81 eV and 1.64 eV using GGA and mBJ-GGA, respectively, at zero pressure. When replacing C by Si, Ge or Sn, we found small narrow gaps that almost touch both valence and conduction bands. These gaps were corrected using the modified Becke-Johnson approximation and the estimated values were in the proximity of 0.5 eV.

LiAlX compounds possess three types of transitions: two of which are indirect along $\Gamma - X$ and $\Gamma - L$ directions and the

last one is direct along $\Gamma - \Gamma$ direction. Unlike the lattice constant, we notice that the $\Gamma - X$ band gaps decrease when going from LiAlC to LiAlSn alloy at zero pressure.

Studying the influence of external pressure on the gap of the crystal structure was also one of the main interests in this paper. For this reason, we have tabulated the variations of the band gaps within different values of pressures for the four LiAlX (X = C, Si, Ge, Sn) compounds in Tables II, III, IV and V, respectively. From these Tables, we notice that these half-Heuslers are characterized by an indirect band gap that does not change for the pressure values considered. Similarly, to LiAlSi, the direct band gap of LiAlSn and LiAlGe compounds is the largest among the three possible transitions at ambient conditions. However, the $\Gamma - \Gamma$ band gap decreases gradually in these alloys with an increase of pressure. For LiAlC,

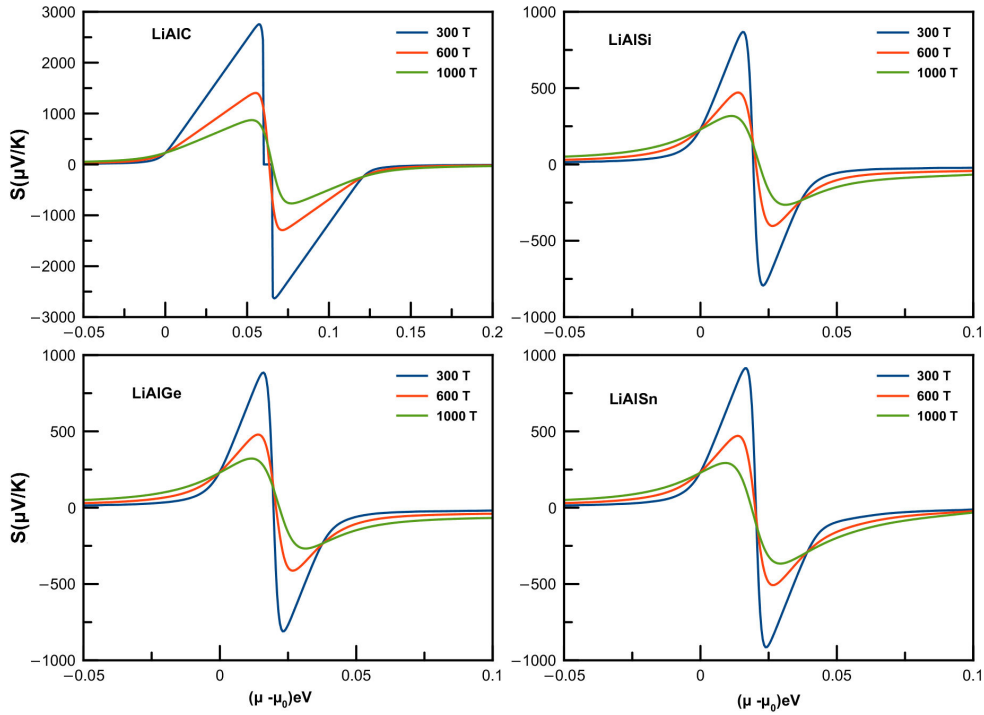


FIGURE 7. The Seebeck coefficient S dependence on chemical potential μ for LiAlX ($X=\text{C}$, Si , Ge , and Sn) compounds at three different temperatures.

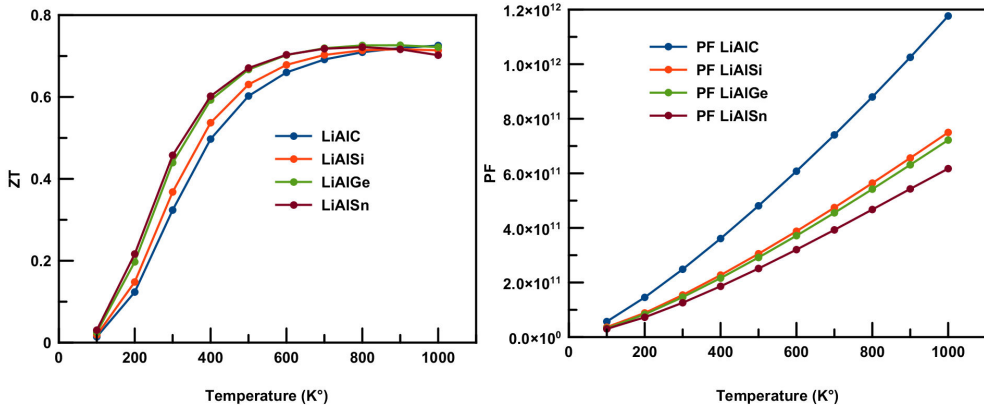


FIGURE 8. Temperature dependence of figure of merit (ZT) and power factor (PF) for LiAlX ($X=\text{C}$, Si , Ge , and Sn) compounds.

the values of the band gap along $\Gamma-L$ direction are the widest at ambient conditions.

The energy gap along $\Gamma-X$ direction decreases for all four compounds with increasing pressure. As for $\Gamma-\Gamma$ and $\Gamma-L$ directions, the band gaps increase for LiAlC , LiAlGe and LiAlSn with increasing pressure (see Table II, IV and V, respectively) and decrease for the LiAlSi alloy (see Table III).

2.2.2. Thermoelectric properties

The Lithium based half-Heusler compounds are known to be very promising in converting heat into power due to their large figure of merit (ZT) [36], which can be expressed as

the following:

$$ZT = \frac{TS^2\sigma}{k_{\text{tot}}}. \quad (1)$$

For this particular reason, we have estimated the Seebeck coefficient S , figure of merit as well as the power factor PF for these LiAlX ($X=\text{C}$, Si , Ge , Sn) compounds, as illustrated in Figs. 7 and 8, respectively.

In the considered range of chemical potential, the Seebeck curve shows almost equal values in both negative and positive regions, meaning that both types of charge carriers may be involved. We notice as well that the large values of thermopower are obtained in low ranges of chemical potential (Fig. 8). The greatest value of the Seebeck reached

2755 $\mu\text{V}\cdot\text{K}^{-1}$ for the LiAlC compound, while LiAlSi, LiAlGe and LiAlSn showed a maximum of 867 $\mu\text{V}\cdot\text{K}^{-1}$, 885 $\mu\text{V}\cdot\text{K}^{-1}$ and 913 $\mu\text{V}\cdot\text{K}^{-1}$, respectively.

When the temperature increases from 300 K to 900 K, the maximum value of thermopower in all four compounds decreases dramatically for both n- and p-type regions.

In order to predict the amount of power generated by the current Li-based materials, we have estimated the variation of the power factor within temperature as can be seen in Fig. 8. The curve of the power factor shows a linear increment with increase of temperature for all four compounds. At 1000 K, LiAlX (X = C, Si, Ge, Sn) compounds show the maximum values $1.18 \times 10^{12} \text{WK}^{-2}\text{m}^{-1}\text{s}^{-1}$, $7.5 \times 10^{11} \text{WK}^{-2}\text{m}^{-1}\text{s}^{-1}$, $7.2 \times 10^{11} \text{WK}^{-2}\text{m}^{-1}\text{s}^{-1}$ and $6.2 \times 10^{11} \text{WK}^{-2}\text{m}^{-1}\text{s}^{-1}$, respectively.

The effective thermal conductivity has a contribution from two parameters namely electronic thermal conductivity k_e and lattice thermal conductivity k_l , where: $k_{tot} = k_e + k_l$. Here, the lattice thermal conductivity k_l was estimated using the Slack equation [37]:

$$k_l = \frac{A\theta_D V^{1/3} m}{\gamma^2 n^{2/3} T},$$

where A is a physical constant ($A \sim 3.1 \times 10^{-6}$), γ is the Grüneisen parameter, θ_D the Debye temperature, V is the volume per atom, n is the number of atoms in the primitive unit cell, and m is the average mass of the atoms in the crystal.

The thermoelectric efficiency of the studied materials was also measured within temperature variation as can be seen in Fig. 7. An exponential increasing behavior is observed in the ZT curve of all compounds. The figure of merit increases sharply with increase of temperature until 700 K, where it shows a slow growth. The maximum values of figure of merit were found to be 0.73 for LiAlC and LiAlGe, and 0.72 for LiAlSi and LiAlSn alloys, respectively. These values correspond to a temperature in the range of 800 to 1000 K.

3. Conclusion

Studying the behavior of the four Li-based systems gave us the opportunity to discover their fascinating properties that might be very useful in different optical and thermoelectric applications. We have first illustrated the band structure and clarified the semiconducting nature of these compounds. Then, we have studied their mechanical stability and calculated the corresponding elastic parameters. All systems remained stable in a moderate range of pressure changes. We have then estimated band gaps of the three possible transitions in each compound under applied forces. LiAlX alloys showed no change of the natural indirect Γ -X gap within pressure variations. In the last part of our investigations, we have been concerned by the thermoelectric efficiency of these Li-based alloys. The Seebeck coefficient of these semiconductors showed that a p-n type of conduction is possible. We found that LiAlX alloys exhibit high values of power factor and figure of merit, which proves their efficiency in the thermoelectric device applications.

Acknowledgments

This work is supported by the Algerian University research project (PRFU) under grant Number B00L02UN220120180018 and the General Directorate for Scientific Research and Technological Development (DGRSDT), Algeria.

Author contributions

Khetir Mohammed: Investigation; resources. Amina Maafa: writing-original draft. Boukabrine Fouzia: Methodology; software; supervision; writing-original draft. Habib Rozale: Supervision. Asma Bouabça: Methodology; software. Abbas Chahed: Methodology; software

1. R. A. de Groot, F. M. Mueller, P. G. van Engen, and K. H. J. Buschow, New Class of Materials: Half-Metallic Ferromagnets, *Phys. Rev. Lett.* **50** (1983) 2024, <https://doi.org/10.1103/PhysRevLett.50.2024>.
2. H. Mehnane *et al.*, First-principles study of new half Heusler for optoelectronic applications. *Superlattices and Microstructures* **51** (2012) 772, <https://doi.org/10.1016/j.spmi.2012.03.020>.
3. D. Kieven, R. Klenk, S. Naghavi, C. Felser, and T. Gruhn, I-II-V half-Heusler compounds for optoelectronics: Ab initio calculations, *Phys. Rev. B* **81** (2010) 075208, <https://doi.org/10.1103/PhysRevB.81.075208>.
4. T. Gruhn, Comparative ab initio study of half-Heusler compounds for optoelectronic applications, *Phys. Rev. B* **82** (2010) 125210, <https://doi.org/10.1103/PhysRevB.82.125210>.
5. F. Shi *et al.*, Hybrid density functional study of bandgaps for 27 new proposed half-Heusler semiconductors, *J. Appl. Phys.* **122** (2017) 215701 <https://doi.org/10.1063/1.4998145>.
6. R. Zhang *et al.*, Two prospective Li-based half-Heusler alloys for spintronic applications based on structural stability and spin-orbit effect, *J. Appl. Phys.* **122** (2017) 013901 <https://doi.org/10.1063/1.4989989>.
7. F. Casper, T. Graf, S. Chadov, B. Balke, C. Felser, Half-Heusler compounds: novel materials for energy and spintronic applications, *Semicond. Sci. Technol.* **27** (2012) 063001. <https://doi.org/10.1088/0268-1242/27/6/063001>.
8. X. Hu, Half-Metallic Antiferromagnet as a Prospective Material for Spintronics, *Adv. Mater.* **24** (2011) 294, <https://doi.org/10.1002/adma.201102555>.

9. J.-W.G. Bos and R.A Downie, Half-Heusler thermoelectrics: a complex class of materials, *J. Phys. Condens. Matter* **26** (2014) 433201, <https://doi.org/10.1088/0953-8984/26/43/433201>.
10. C. Felser and A. Hirohata, *Heusler Alloys* (Springer, Cham, 2016), <https://doi.org/10.1007/978-3-319-21449-8>.
11. A. Erkisi, G. Surucu, and R. Ellialtioglu, The investigation of electronic, mechanical and lattice dynamical properties of PdCoX (X=Si and Ge) half-Heusler metallics in α , β and γ structural phases: an ab initio study, *Phil. Mag* **97** (2017) 2237, <https://doi.org/10.1080/14786435.2017.1329595>.
12. W. Kohn and L. Sham, Self-Consistent Equations Including Exchange and Correlation Effects, *Phys. Rev.* **140** (1965) A1133 <https://doi.org/10.1103/PhysRev.140.A1133>.
13. N. Belmiloud, F. Boutaiba, A. Belabbes, M. Ferhat, and F. Bechstedt, Half-Heusler compounds with a 1 eV (1.7 eV) direct band gap, lattice-matched to GaAs (Si), for solar cell application: A first-principles study, *Phys. Status Solidi B* **253** (2016) 889. <https://doi.org/10.1002/pssb.201552674>.
14. S. Yousuf and D.C. Gupta, Thermoelectric response of Zr-NiSn and ZrNiPb Half-Heuslers: Applicability of semi-classical Boltzmann transport theory, *Results Phys* **12** (2019) 1382. <https://doi.org/10.1016/j.rinp.2019.01.026>.
15. D.J. Singh and L. Nordström, *Planewaves, Pseudopotential and the LAPW Method*, (Springer, Boston 1994). <https://doi.org/10.1007/978-0-387-29684-5>.
16. M. Weinert, E. Wimmer, and A. Freeman, Total-energy all-electron density functional method for bulk solids and surfaces, *Phys. Rev. B* **26** (1982) 4571. <https://doi.org/10.1103/PhysRevB.26.4571>.
17. E. Wimmer, H. Krakauer, M. Weinert, and A. J. Freeman, Freeman A Full-potential self-consistent linearized-augmented-plane-wave method for calculating the electronic structure of molecules and surfaces: O_2 molecule, *Phys. Rev. B* **24** (1981) 864. <https://doi.org/10.1103/PhysRevB.24.864>.
18. P. Blaha *et al.*, WIEN2K: An augmented plane wave plus local orbitals program for calculating crystal properties, Vienna University of Technology, 2001.
19. J.P. Perdew and Y. Wang, Accurate and simple analytic representation of the electron-gas correlation energy, *Phys. Rev. B* **45** (1992) 13244. <https://doi.org/10.1103/PhysRevB.45.13244>.
20. J.P. Perdew, K. Burke, and M. Ernzerhof, Generalized Gradient Approximation Made Simple, *Phys. Rev. Lett* **77** (1996) 3865. <https://doi.org/10.1103/PhysRevLett.77.3865>.
21. A.D. Becke and E.R. Johnson, A simple effective potential for exchange, *J. Chem. Phys* **124** (2006) 221101. <https://doi.org/10.1063/1.2213970>.
22. F.D. Murnaghan, The Compressibility of Media under Extreme Pressures, *Proc. Natl. Acad. Sci. U. S. A* **30** (1944) 244. <https://doi.org/10.1073/pnas.30.9.244>.
23. S.A. Sofi and D.C. Gupta, High temperature and pressure dependent structural and thermophysical properties of Co_2VN (N = Sn, Sb) ferromagnetic materials, *Mater. Res. Express* **7** (2020) 125701, <https://doi.org/10.1088/2053-1591/abcfd5>.
24. T. Charpin, A package for calculating elastic tensors of cubic phases using WIEN, Laboratory of Geomaterials IPGP, 2001.
25. G.K.H. Madsen and D.J. Singh, BoltzTraP. A code for calculating band-structure dependent quantities, *Comput. Phys. Commun.* **175** (2006) 67, <https://doi.org/10.1016/j.cpc.2006.03.007>.
26. H. Nowotny and F. Holub, Untersuchungen an metallischen Systemen mit Flußspatphasen. *Monatsh. Chem.* **91** (1960) 877. <https://doi.org/10.1007/BF00929560>.
27. S. H. Shah, S. H. Khan, A. Laref, and Murtaza, Optoelectronic and transport properties of LiBZ (B = Al, In, Ga and Z = Si, Ge, Sn) semiconductors, *J. Solid State Chem.* **258** (2018) 800, <https://doi.org/10.1016/j.jssc.2017.12.014>.
28. M. Born and K. Huang, *Dynamical Theory of Crystal Lattices*, (Clarendon Press, Oxford, 1954).
29. N. Erum and M. A. Iqbal, Effect of hydrostatic pressure on physical properties of strontium based fluoroperovskites for novel applications, *Mater. Res. Express* **5** (2018) 025904, <https://doi.org/10.1088/2053-1591/aaad5c>.
30. O. Gomis *et al.*, High-pressure structural and elastic properties of Tl_2O_3 , *J. Appl. Phys* **116** (2014) 133521 <https://doi.org/10.1088/2053-1591/aaad5c>.
31. S.F. Pugh, XCII. Relations between the elastic moduli and the plastic properties of polycrystalline pure metals, Lond. Edinb. Dublin Philos. Mag. J. Sci. **45** (1954) 823, <https://doi.org/10.1080/14786440808520496>.
32. R. Hill, The Elastic Behaviour of a Crystalline Aggregate, *Proc. Phys. Soc. A.* **65** (1952) 349. <https://doi.org/10.1088/0370-1298/65/5/307>.
33. P. Mao, B. Yu, Z. Liu, F. Wang, and Y. Ju, First-principles investigation on mechanical, electronic, and thermodynamic properties of Mg_2Sr under high pressure, *J. Appl. Phys* **117** (2015) 115903, <https://doi.org/10.1063/1.4915339>.
34. C. M. Zener and S. Zener, Elasticity and anelasticity of metals. *J. Phys. Chem.* **53** (1949) 1468, <https://doi.org/10.1021/j150474a017>.
35. S. Kacimi, H. Mehnane, and A. Zaoui, I-II-V and I-III-IV half-Heusler compounds for optoelectronic applications: Comparative ab initio study, *J. Alloys Compd.* **587** (2014) 451 <https://doi.org/10.1016/j.jallcom.2013.10.046>.
36. R.P. Chasmar and R. Stratton, The Thermoelectric Figure of Merit and its Relation to Thermoelectric Generators, *J. Electron. Control*, **7** (1959) 52. <https://doi.org/10.1080/00207215908937186>.
37. J. W. F. Dorleijn, Electrical conduction in ferromagnetic metals, *Philips Res. Rep.* **31** (1976) 287.